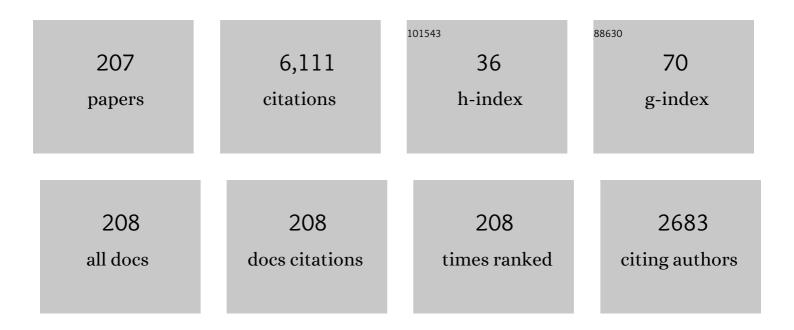
motomichi koyama

List of Publications by Year in descending order

Source: https://exaly.com/author-pdf/4792569/publications.pdf Version: 2024-02-01



MOTOMICHI KOYAMA

#	Article	IF	CITATIONS
1	Pre-straining alters hydrogen-assisted cracking site and local hydrogen diffusivity in a nitrogen-doped duplex steel. Scripta Materialia, 2022, 207, 114272.	5.2	9
2	Realâ€Time Visualization of Hydrogen Distribution in Metals Using Polyaniline: An Ultrasensitive Hydrogenochromic Sensor. Advanced Materials Interfaces, 2022, 9, .	3.7	5
3	Synergistic effects of hydrogen and deformation temperature on mechanical properties of TRIP-aided bainitic ferrite steel. Materials Science & Engineering A: Structural Materials: Properties, Microstructure and Processing, 2022, 842, 143070.	5.6	6
4	Hydrogen-accelerated fatigue crack growth of equiatomic Fe–Cr–Ni–Mn–Co high-entropy alloy evaluated by compact tension testing. Materials Science & Engineering A: Structural Materials: Properties, Microstructure and Processing, 2022, 848, 143394.	5.6	5
5	Transition mechanism of cycle- to time-dependent acceleration of fatigue crack-growth in 0.4Â%C Cr-Mo steel in a pressurized gaseous hydrogen environment. International Journal of Fatigue, 2022, 163, 107039.	5.7	14
6	Three-dimensional characterization of low-cycle fatigue crack morphology in TRIP-maraging steel: Crack closure, geometrical uncertainty and wear. International Journal of Fatigue, 2021, 143, 106032.	5.7	1
7	Hydrogen-assisted damage evolution in nitrogen-doped duplex stainless steel. International Journal of Hydrogen Energy, 2021, 46, 2716-2728.	7.1	7
8	Novel â^'75°C SEM cooling stage: application for martensitic transformation in steel. Microscopy (Oxford, England), 2021, 70, 250-254.	1.5	1
9	Effects of Matrix Structure and Nitrogen Content on Fatigue Properties of Ultrahigh-Strength Low Alloy TRIP-Aided Steels. ISIJ International, 2021, 61, 591-598.	1.4	2
10	Fatigue Crack Growth at Different Frequencies and Temperatures in an Fe-based Metastable High-entropy Alloy. ISIJ International, 2021, 61, 641-647.	1.4	7
11	Stacking fault aggregation during cooling composing FCC–HCP martensitic transformation revealed by <i>in-situ</i> electron channeling contrast imaging in an Fe-high Mn alloy. Science and Technology of Advanced Materials, 2021, 22, 135-140.	6.1	5
12	Microstructure Refinement by Low-Temperature Ausforming in an Fe-Based Metastable High-Entropy Alloy. Metals, 2021, 11, 742.	2.3	2
13	Effect of austempering treatment on the microstructure and mechanical properties of 0.4C–1.5Si-1.5Mn TRIP-aided bainitic ferrite steel. Materials Science & Engineering A: Structural Materials: Properties, Microstructure and Processing, 2021, 819, 141479.	5.6	17
14	Strain rate sensitivity of hydrogen-assisted ε-martensitic transformation and associated hydrogen embrittlement in high-Mn steel. International Journal of Hydrogen Energy, 2021, 46, 27221-27233.	7.1	13
15	Hierarchical Characteristics of Hydrogen-Assisted Crack Growth and Microstructural Strain Evolution in Tempered Martensitic Steels: Case of Quasi-cleavage Fracture. Metallurgical and Materials Transactions A: Physical Metallurgy and Materials Science, 2021, 52, 4703-4713.	2.2	11
16	Hydrogenation treatment under several gigapascals assists diffusionless transformation in a face-centered cubic steel. Scientific Reports, 2021, 11, 19384.	3.3	4
17	Hydrogen embrittlement and associated surface crack growth in fine-grained equiatomic CoCrFeMnNi high-entropy alloys with different annealing temperatures evaluated by tensile testing under in situ hydrogen charging. International Journal of Hydrogen Energy, 2021, 46, 33028-33038.	7.1	16
18	Depressurization-induced diffusionless transformation in pure iron hydrogenated under several gigapascals. Materials Letters: X, 2021, 11, 100078.	0.7	1

#	Article	IF	CITATIONS
19	Notch shape dependence of fatigue crack extension in equiatomic CrMnFeCoNi high-entropy alloy. International Journal of Fatigue, 2021, 153, 106481.	5.7	7
20	Quantification and Characterization of Microdamage Resistance in Metals for Designing High-Strength Ductile Microstructures. Accounts of Materials Research, 2021, 2, 1167-1176.	11.7	7
21	Planar slip-driven fatigue crack initiation and propagation in an equiatomic CrMnFeCoNi high-entropy alloy. International Journal of Fatigue, 2020, 133, 105418.	5.7	55
22	Strain rate and hydrogen effects on crack growth from a notch in a Fe-high-Mn steel containing 1.1Âwt% solute carbon. International Journal of Hydrogen Energy, 2020, 45, 1125-1139.	7.1	19
23	Plastic deformation sequence and strain gradient characteristics of hydrogen-induced delayed crack propagation in single-crystalline Fe–Si alloy. Scripta Materialia, 2020, 178, 99-103.	5.2	7
24	Quantitative Evaluation of Hydrogen Effects on Evolutions of Deformation-Induced ε-Martensite and Damage in a High-Mn Steel. Metallurgical and Materials Transactions A: Physical Metallurgy and Materials Science, 2020, 51, 6184-6194.	2.2	14
25	Shallow crack effect on evaluation of residual tensile strength: Harmless and stable cracks in finite-sized structure made of ductile metals. Theoretical and Applied Fracture Mechanics, 2020, 109, 102734.	4.7	4
26	Pre-strain effects on critical stress and hydrogen content for hydrogen-induced quasi-cleavage fracture in a TRIP-aided bainitic ferrite steel: Martensitic transformation, matrix damage, and strain aging. International Journal of Hydrogen Energy, 2020, 45, 27920-27928.	7.1	17
27	Effects of Mn Content and Grain Size on Hydrogen Embrittlement Susceptibility of Face-Centered Cubic High-Entropy Alloys. Metallurgical and Materials Transactions A: Physical Metallurgy and Materials Science, 2020, 51, 5612-5616.	2.2	30
28	Application of an iridium complex for detecting hydrogen permeation through pure iron. International Journal of Hydrogen Energy, 2020, 45, 25580-25586.	7.1	12
29	Distinguishing geometric and metallurgic hydrogen-embrittlement susceptibilities in pre-cracked structures made of interstitial-free steel under monotonic tension. Theoretical and Applied Fracture Mechanics, 2020, 108, 102574.	4.7	1
30	Hydrogen Enhances Shape Memory Effect of a Ferrous Face-Centered Cubic Alloy. Metallurgical and Materials Transactions A: Physical Metallurgy and Materials Science, 2020, 51, 4439-4441.	2.2	6
31	Effects of hydrogen content that alters damage evolution mechanisms in SUH 660 precipitation-strengthened Fe–Cr–Ni steel. Materials Science & Engineering A: Structural Materials: Properties, Microstructure and Processing, 2020, 791, 139750.	5.6	4
32	Origin of micrometer-scale dislocation motion during hydrogen desorption. Science Advances, 2020, 6, eaaz1187.	10.3	29
33	Hydrogen embrittlement resistance of pre-strained ultra-high-strength low alloy TRIP-aided steel. International Journal of Fracture, 2020, 224, 253-260.	2.2	18
34	Simplified stress field determination for an inclined crack and interaction between two cracks under tension. Theoretical and Applied Fracture Mechanics, 2020, 107, 102561.	4.7	8
35	Understanding the damage initiation mechanism of precipitation-strengthened Fe-Ni-Cr based austenitic steel. Materials Today: Proceedings, 2020, 26, 3081-3084.	1.8	0
36	Gaseous hydrogen embrittlement of a Ni-free austenitic stainless steel containing 1 mass% nitrogen: Effects of nitrogen-enhanced dislocation planarity. International Journal of Hydrogen Energy, 2020, 45, 10209-10218.	7.1	30

#	Article	IF	CITATIONS
37	Fundamental criterion Ktrans for failure analysis of hydrogen-assisted cracks in notched specimens of pure Ni. Theoretical and Applied Fracture Mechanics, 2020, 107, 102556.	4.7	4
38	Fatigue crack propagation modes: plastic deformation mode and damage accumulation mode. International Journal of Fracture, 2020, 222, 111-122.	2.2	14
39	Equivalence between shallow notch and shallow crack in structural failure caused by plastic instability. Theoretical and Applied Fracture Mechanics, 2020, 108, 102577.	4.7	Ο
40	Growth Behavior of a Mechanically Long Fatigue Crack in an FeCrNiMnCo High Entropy Alloy: A Comparison with an Austenitic Stainless Steel. ISIJ International, 2020, 60, 175-181.	1.4	13
41	Multiple damage mechanisms facilitated by planar dislocation glide in a commercial-grade precipitation-strengthened Fe–Ni–Cr-based steel. Materials Science & Engineering A: Structural Materials: Properties, Microstructure and Processing, 2020, 782, 139250.	5.6	8
42	Influence of dynamic-strain aging due to excess Mg on fatigue crack growth rate scatter in Al6061-T6 alloy. Theoretical and Applied Fracture Mechanics, 2020, 108, 102617.	4.7	2
43	Data of dynamic microscale strain distributions of Ti-6Al-4V alloys in dwell fatigue tests. Data in Brief, 2019, 25, 104338.	1.0	3
44	Crystallographic selection rule for the propagation mode of microstructurally small fatigue crack in a laminated Ti-6Al-4V alloy: Roles of basal and pyramidal slips. International Journal of Fatigue, 2019, 128, 105200.	5.7	25
45	Dislocation motion at a fatigue crack tip in a high-nitrogen steel clarified through in situ electron channeling contrast imaging. Materials Characterization, 2019, 158, 109930.	4.4	16
46	A patient-specific numerical modeling of the spontaneous coronary artery dissection in relation to atherosclerosis. Computer Methods and Programs in Biomedicine, 2019, 182, 105060.	4.7	7
47	Mode I fatigue crack growth induced by strain-aging in precipitation-hardened aluminum alloys. Theoretical and Applied Fracture Mechanics, 2019, 104, 102340.	4.7	11
48	Transformation-assisted hydrogen desorption during deformation in steels: Examples of α′- and ε-Martensite. International Journal of Hydrogen Energy, 2019, 44, 30472-30477.	7.1	23
49	Effect analysis of stress-intensity-factor-range decreasing rate for obtaining threshold stress-intensity-factor-range. Theoretical and Applied Fracture Mechanics, 2019, 104, 102377.	4.7	1
50	Detection of hydrogen effusion before, during, and after martensitic transformation: Example of multiphase transformation-induced plasticity steel. International Journal of Hydrogen Energy, 2019, 44, 26028-26035.	7.1	12
51	EBSD and ECCI Based Assessments of Inhomogeneous Plastic Strain Evolution Coupled with Digital Image Correlation. Tetsu-To-Hagane/Journal of the Iron and Steel Institute of Japan, 2019, 105, 222-230.	0.4	10
52	Fatigue Behavior in an Fe–N Binary Ferritic Steel: Similarity and Difference between Carbon and Nitrogen. ISIJ International, 2019, 59, 186-191.	1.4	3
53	Strain-rate sensitivity of hydrogen-assisted damage evolution and failure in dual-phase steel: From vacancy to micrometer-scale void growth. Engineering Fracture Mechanics, 2019, 216, 106513.	4.3	10
54	Grain refinement effect on hydrogen embrittlement resistance of an equiatomic CoCrFeMnNi high-entropy alloy. International Journal of Hydrogen Energy, 2019, 44, 17163-17167.	7.1	51

#	Article	IF	CITATIONS
55	Revisiting the effects of hydrogen on deformation-induced Î ³ -ε martensitic transformation. Materials Letters, 2019, 249, 197-200.	2.6	22
56	1-second-resolved strain mapping in Ti-6Al-4V alloys during dwell fatigue in SEM by video sampling moiré. Mechanics of Materials, 2019, 133, 63-70.	3.2	9
57	Enhancement of hydrogen embrittlement resistance of Fe-Mn-C twinning-induced plasticity steel by partial recrystallization technique. Materials Characterization, 2019, 151, 221-226.	4.4	8
58	Overview of metastability and compositional complexity effects for hydrogen-resistant iron alloys: Inverse austenite stability effects. Engineering Fracture Mechanics, 2019, 214, 123-133.	4.3	33
59	Growth Behavior of a Mechanically Long Fatigue Crack in an FeCrNiMnCo High Entropy Alloy: A Comparison with an Austenitic Stainless Steel. Tetsu-To-Hagane/Journal of the Iron and Steel Institute of Japan, 2019, 105, 215-221.	0.4	7
60	Influence of Stress Re-distribution on Hydrogen-induced Fatigue Crack Propagation. ISIJ International, 2019, 59, 1683-1690.	1.4	3
61	EBSD- and ECCI-based Assessments of Inhomogeneous Plastic Strain Evolution Coupled with Digital Image Correlation. ISIJ International, 2019, 59, 2334-2342.	1.4	14
62	Resistance to mechanically small fatigue crack growth in ultrafine grained interstitial-free steel fabricated by accumulative roll-bonding. International Journal of Fatigue, 2019, 118, 117-125.	5.7	13
63	Phase Stability Effects on Hydrogen Embrittlement Resistance in Martensite–Reverted Austenite Steels. Metallurgical and Materials Transactions A: Physical Metallurgy and Materials Science, 2019, 50, 29-34.	2.2	12
64	Lowering Strain Rate Simultaneously Enhances Carbon- and Hydrogen-Induced Mechanical Degradation in an Fe-33Mn-1.1C Steel. Metallurgical and Materials Transactions A: Physical Metallurgy and Materials Science, 2019, 50, 1137-1141.	2.2	12
65	Fatigue Resistance of Laminated and Non-laminated TRIP-maraging Steels: Crack Roughness vs Tensile Strength. Metallurgical and Materials Transactions A: Physical Metallurgy and Materials Science, 2019, 50, 1142-1145.	2.2	8
66	ECCI Characterization of Dislocation Structures at a Non-propagating Fatigue Crack Tip: Toward Understanding the Effects of Mn-C and Cr-N Couples on Crack Growth Resistance. Metallurgical and Materials Transactions A: Physical Metallurgy and Materials Science, 2019, 50, 426-435.	2.2	9
67	Microstructural mechanisms of fatigue crack non-propagation in TRIP-maraging steels. International Journal of Fatigue, 2018, 113, 126-136.	5.7	23
68	High-concentration carbon assists plasticity-driven hydrogen embrittlement in a Fe-high Mn steel with a relatively high stacking fault energy. Materials Science & Engineering A: Structural Materials: Properties, Microstructure and Processing, 2018, 717, 78-84.	5.6	18
69	Interstitial Carbon Enhanced Corrosion Resistance of Fe-33Mn-xC Austenitic Steels: Inhibition of Anodic Dissolution. Journal of the Electrochemical Society, 2018, 165, C19-C26.	2.9	16
70	On the Utility of Crystal Plasticity Modeling to Uncover the Individual Roles of Microdeformation Mechanisms on the Work Hardening Response of Fe-23Mn-0.5C TWIP Steel in the Presence of Hydrogen. Journal of Engineering Materials and Technology, Transactions of the ASME, 2018, 140, .	1.4	4
71	Hydrogen-assisted failure in a bimodal twinning-induced plasticity steel: Delamination events and damage evolution. International Journal of Hydrogen Energy, 2018, 43, 2492-2502.	7.1	15
72	Temperature dependence of transgranular fatigue crack resistance in interstitial-free steel and Fe-C steels with supersaturated carbon: Effects of dynamic strain aging and dynamic precipitation. International Journal of Fatigue, 2018, 110, 1-9.	5.7	12

#	Article	IF	CITATIONS
73	Non-propagating fatigue cracks in austenitic steels with a micro-notch: Effects of dynamic strain aging, martensitic transformation, and microstructural hardness heterogeneity. International Journal of Fatigue, 2018, 113, 359-366.	5.7	12
74	Comparative study of hydrogen embrittlement in stable and metastable high-entropy alloys. Scripta Materialia, 2018, 150, 74-77.	5.2	84
75	Micrographic Digital Image Correlation Coupled with Microlithography: Case Study of Strain Localization and Subsequent Cracking at an FIB Notch Tip in a Laminated Ti-6Al-4V Alloy. Experimental Mechanics, 2018, 58, 381-386.	2.0	12
76	Visualization of dislocations through electron channeling contrast imaging at fatigue crack tip, interacting with pre-existing dislocations. Materials Research Letters, 2018, 6, 61-66.	8.7	19
77	Microstructural hardness heterogeneity triggers fatigue crack non-propagation in as-hot-rolled Fe-30Mn-3Si-3Al twinning-induced plasticity steel. International Journal of Fatigue, 2018, 108, 18-24.	5.7	12
78	Fatigue Behavior of Fe-Cr-Ni-based Metastable Austenitic Steels with an Identical Tensile Strength and Different Solute Carbon Contents. ISIJ International, 2018, 58, 1910-1919.	1.4	5
79	Fatigue Behavior of Fe-Cr-Ni-based Metastable Austenitic Steels with an Identical Tensile Strength and Different Solute Carbon Contents. Tetsu-To-Hagane/Journal of the Iron and Steel Institute of Japan, 2018, 104, 88-97.	0.4	1
80	A new design concept for prevention of hydrogen-induced mechanical degradation: viewpoints of metastability and high entropy. Procedia Structural Integrity, 2018, 13, 292-297.	0.8	8
81	Crystallographic orientation-dependent growth mode of microstructurally fatigue small crack in a laminated Ti–6Al–4V alloy. Procedia Structural Integrity, 2018, 13, 694-699.	0.8	5
82	Localized Plasticity and Associated Cracking in Stable and Metastable High-Entropy Alloys Pre-Charged with Hydrogen. Procedia Structural Integrity, 2018, 13, 716-721.	0.8	12
83	Fatigue Crack Growth Behavior and Associated Microstructure in a Metastable High-Entropy Alloy. Procedia Structural Integrity, 2018, 13, 831-836.	0.8	15
84	Re-examination of fatigue crack propagation mechanism under cyclic Mode II loading. Procedia Structural Integrity, 2018, 13, 1026-1031.	0.8	4
85	Effect of Si on temperature dependence of non-propagation limit of small fatigue crack in a Fe-C alloy. Procedia Structural Integrity, 2018, 13, 1032-1036.	0.8	3
86	Small fatigue crack growth in a high entropy alloy. Procedia Structural Integrity, 2018, 13, 1065-1070.	0.8	11
87	Quantification method for parameters affecting multi-scale roughness-induced fatigue crack closure. Procedia Structural Integrity, 2018, 13, 1071-1075.	0.8	2
88	Proposal of fractographic analysis method coupled with EBSD and ECCI. Procedia Structural Integrity, 2018, 13, 1076-1081.	0.8	3
89	Analysis of fatigue crack configuration influence on fatigue life. Procedia Structural Integrity, 2018, 13, 1148-1153.	0.8	2
90	Strain Rate Sensitivity of Microstructural Damage Evolution in a Dual-Phase Steel Pre-Charged with Hydrogen. Procedia Structural Integrity, 2018, 13, 710-715.	0.8	4

#	Article	lF	CITATIONS
91	The influence of fracture surface contact in fatigue crack propagation of material having texture under Mode II loading. Procedia Structural Integrity, 2018, 13, 1088-1092.	0.8	0
92	Proposal and verification of novel fatigue crack propagation simulation method by finite element method Procedia Structural Integrity, 2018, 13, 1154-1158.	0.8	1
93	Influence of shear-affected-zone due to punching on tensile characteristics of steel plate. Procedia Structural Integrity, 2018, 13, 1047-1052.	0.8	0
94	Overview of Dynamic Strain Aging and Associated Phenomena in Fe–Mn–C Austenitic Steels. ISIJ International, 2018, 58, 1383-1395.	1.4	47
95	Split and Shift of <i>ε</i> -martensite Peak in an X-ray Diffraction Profile during Hydrogen Desorption: A Geometric Effect of Atomic Sequence. ISIJ International, 2018, 58, 1745-1747.	1.4	3
96	An unconventional hydrogen effect that suppresses thermal formation of the hcp phase in fcc steels. Scientific Reports, 2018, 8, 16136.	3.3	15
97	Overview of Dynamic Strain Aging and Associated Phenomena in Fe-Mn-C Austenitic Steels. Tetsu-To-Hagane/Journal of the Iron and Steel Institute of Japan, 2018, 104, 187-200.	0.4	6
98	Optical Microscopy-Based Damage Quantification: an Example of Cryogenic Deformation of a Dual-Phase Steel. ISIJ International, 2018, 58, 179-185.	1.4	12
99	Optical full-field strain measurement method from wrapped sampling Moiré phase to minimize the influence of defects and its applications. Optics and Lasers in Engineering, 2018, 110, 155-162.	3.8	27
100	Effect of state of carbon on fatigue properties and dislocation structure of Fe-0.017mass%C alloy. Materials Science & Engineering A: Structural Materials: Properties, Microstructure and Processing, 2018, 732, 212-219.	5.6	6
101	First-Principles Study on Hydrogen Diffusivity in BCC, FCC, and HCP Iron. Metallurgical and Materials Transactions A: Physical Metallurgy and Materials Science, 2018, 49, 5015-5022.	2.2	63
102	Influence of Stress Re-distribution on Hydrogen-induced Fatigue Crack Propagation. Tetsu-To-Hagane/Journal of the Iron and Steel Institute of Japan, 2018, 104, 46-53.	0.4	0
103	Microstructural damage evolution and arrest in binary Fe–high-Mn alloys with different deformation temperatures. International Journal of Fracture, 2018, 213, 193-206.	2.2	9
104	Ductile-to-brittle transition in tensile failure due to shear-affected zone with a stress-concentration source: a comparative study on punched-plate tensile-failure characteristics of precipitation-hardened and dual-phase steels. International Journal of Fracture, 2018, 212, 237-248.	2.2	9
105	Effect of shear-affected zone on fatigue crack propagation mode. International Journal of Fatigue, 2018, 116, 36-47.	5.7	8
106	Surface orientation dependence of hydrogen flux in lenticular martensite of an Fe-Ni-C alloy clarified through in situ silver decoration technique. Materials Letters, 2018, 228, 273-276.	2.6	5
107	Roughness-induced stress shielding effect in fatigue crack propagation under Mode II loading. International Journal of Fatigue, 2018, 116, 245-256.	5.7	12
108	Underlying interstitial carbon concentration dependence of transgranular fatigue crack resistance in Fe-C ferritic steels: The kinetic effect viewpoint. International Journal of Fatigue, 2017, 98, 101-110.	5.7	23

#	Article	IF	CITATIONS
109	Bone-like crack resistance in hierarchical metastable nanolaminate steels. Science, 2017, 355, 1055-1057.	12.6	297
110	Impact of Mn–C couples on fatigue crack growth in austenitic steels: Is the attractive atomic interaction negative or positive?. International Journal of Fatigue, 2017, 99, 1-12.	5.7	21
111	Multiscale in situ deformation experiments: A sequential process from strain localization to failure in a laminated Ti-6Al-4V alloy. Materials Characterization, 2017, 128, 217-225.	4.4	14
112	Effects of martensitic transformability and dynamic strain age hardenability on plasticity in metastable austenitic steels containing carbon. Journal of Materials Science, 2017, 52, 7868-7882.	3.7	38
113	Material property controlling non-propagating fatigue crack length of mechanically and physically short-crack based on Dugdale-model analysis. Theoretical and Applied Fracture Mechanics, 2017, 90, 193-202.	4.7	8
114	Mechanical-probabilistic evaluation of size effect of fatigue life using data obtained from single smooth specimen: An example using Fe-30Mn-4Si-2Al seismic damper alloy. Engineering Failure Analysis, 2017, 72, 34-47.	4.0	11
115	Recent progress in microstructural hydrogen mapping in steels: Quantification, kinetic analysis, and multi-scale characterisation. Materials Science and Technology, 2017, 33, 1481-1496.	1.6	125
116	Characteristics of hydrogen-assisted intergranular fatigue crack growth in interstitial-free steel: role of plastic strain localization. International Journal of Fracture, 2017, 206, 123-130.	2.2	19
117	Effects of lamella size and connectivity on fatigue crack resistance of TRIP-maraging steel. International Journal of Fatigue, 2017, 100, 176-186.	5.7	19
118	Overview of hydrogen embrittlement in high-Mn steels. International Journal of Hydrogen Energy, 2017, 42, 12706-12723.	7.1	228
119	Hydrogen desorption and cracking associated with martensitic transformation in Fe-Cr-Ni-Based austenitic steels with different carbon contents. International Journal of Hydrogen Energy, 2017, 42, 26423-26435.	7.1	39
120	Fatigue crack non-propagation assisted by nitrogen-enhanced dislocation planarity in austenitic stainless steels. International Journal of Fatigue, 2017, 104, 158-170.	5.7	13
121	Room-temperature blue brittleness of Fe-Mn-C austenitic steels. Scripta Materialia, 2017, 141, 20-23.	5.2	37
122	Reply to comments on the paper "In situ observations of silver-decoration evolution under hydrogen permeation: Effects of grain boundary misorientation on hydrogen flux in pure iron―by Gavriljuk and Teus. Scripta Materialia, 2017, 140, 91-92.	5.2	5
123	Threshold stress intensity factor range of a mechanically-long and microstructually-short crack perpendicular to an interface with plastic mismatch. Engineering Fracture Mechanics, 2017, 182, 287-302.	4.3	11
124	Effects of ε-martensitic transformation on crack tip deformation, plastic damage accumulation, and slip plane cracking associated with low-cycle fatigue crack growth. International Journal of Fatigue, 2017, 103, 533-545.	5.7	27
125	Effect of the state of carbon on ductility in Fe-0.017mass%C ferritic steel. Materials Science & Engineering A: Structural Materials: Properties, Microstructure and Processing, 2017, 701, 120-128.	5.6	9
126	In situ observations of silver-decoration evolution under hydrogen permeation: Effects of grain boundary misorientation on hydrogen flux in pure iron. Scripta Materialia, 2017, 129, 48-51.	5.2	66

#	Article	IF	CITATIONS
127	Generalized evaluation method for determining transition crack length for microstructurally small to microstructurally large fatigue crack growth: Experimental definition, facilitation, and validation. International Journal of Fatigue, 2017, 95, 38-44.	5.7	14
128	Comparative study on small fatigue crack propagation between Fe-30Mn-3Si-3Al and Fe-23Mn-0.5C twinning-induced plasticity steels: Aspects of non-propagation of small fatigue cracks. International Journal of Fatigue, 2017, 94, 1-5.	5.7	27
129	Interfacial hydrogen localization in austenite/martensite dualâ€phase steel visualized through optimized silver decoration and scanning Kelvin probe force microscopy. Materials and Corrosion - Werkstoffe Und Korrosion, 2017, 68, 306-310.	1.5	20
130	Two-dimensional Moiré phase analysis for accurate strain distribution measurement and application in crack prediction. Optics Express, 2017, 25, 13465.	3.4	38
131	Intrinsic Factors that Trigger the Coaxing Effect in Binary Fe–C Ferritic Alloys with a Focus on Strain Aging. ISIJ International, 2017, 57, 358-364.	1.4	10
132	Intrinsic Factors That Trigger the Coaxing Effect in Binary Fe-C Ferritic Alloys with a Focus on Strain Aging. Tetsu-To-Hagane/Journal of the Iron and Steel Institute of Japan, 2017, 103, 660-666.	0.4	3
133	Characteristic Fatigue Crack Growth Behavior of Low Carbon Steel under Low-pressure Hydrogen Gas Atmosphere in an Ultra-low Frequency. ISIJ International, 2016, 56, 855-860.	1.4	8
134	Suppression Mechanism of Strain-age-hardening in Carbon Steel Associated with Hydrogen Uptake. ISIJ International, 2016, 56, 1656-1661.	1.4	6
135	Combined Multi-scale Analyses on Strain/Damage/Microstructure in Steel: Example of Damage Evolution Associated with lµ-martensitic Transformation. Tetsu-To-Hagane/Journal of the Iron and Steel Institute of Japan, 2016, 102, 227-236.	0.4	6
136	Notch Sensitivity of the Fatigue Limit in High-Strength Steel. ISIJ International, 2016, 56, 1480-1486.	1.4	8
137	Combined Multi-scale Analyses on Strain/Damage/Microstructure in Steel: Example of Damage Evolution Associated with <i>ε</i> -martensitic Transformation. ISIJ International, 2016, 56, 2037-2046.	1.4	25
138	Effect of strain rate on hydrogen embrittlement susceptibility of twinning-induced plasticity steel pre-charged with high-pressure hydrogen gas. International Journal of Hydrogen Energy, 2016, 41, 15362-15372.	7.1	79
139	Martensitic transformation-induced hydrogen desorption characterized by utilizing cryogenic thermal desorption spectroscopy during cooling. Scripta Materialia, 2016, 122, 50-53.	5.2	34
140	In situ microscopic observations of low-cycle fatigue-crack propagation in high-Mn austenitic alloys with deformation-induced ε-martensitic transformation. Acta Materialia, 2016, 112, 326-336.	7.9	61
141	Hexagonal close-packed Martensite-related Fatigue Crack Growth under the Influence of Hydrogen: Example of Fe–15Mn–10Cr–8Ni–4Si Austenitic Alloy. Scripta Materialia, 2016, 113, 6-9.	5.2	17
142	Elucidation of the effects of cementite morphology on damage formation during monotonic and cyclic tension in binary low carbon steels using in situ characterization. Materials Science & Engineering A: Structural Materials: Properties, Microstructure and Processing, 2016, 667, 358-367.	5.6	13
143	Hydrogen Embrittlement Susceptibility of Fe-Mn Binary Alloys with High Mn Content: Effects of Stable and Metastable Îμ-Martensite, and Mn Concentration. Metallurgical and Materials Transactions A: Physical Metallurgy and Materials Science, 2016, 47, 2656-2673.	2.2	67
144	Potential resistance to transgranular fatigue crack growth of Fe–C alloy with a supersaturated carbon clarified through FIB micro-notching technique. International Journal of Fatigue, 2016, 87, 1-5.	5.7	30

#	Article	IF	CITATIONS
145	Hydrogen-assisted damage in austenite/martensite dual-phase steel. Philosophical Magazine Letters, 2016, 96, 9-18.	1.2	25
146	Intergranular Fatigue Crack Initiation and its Associated Small Fatigue Crack Propagation in Water-quenched Fe-C Fully Ferritic Steel. Tetsu-To-Hagane/Journal of the Iron and Steel Institute of Japan, 2016, 102, 268-273.	0.4	6
147	Importance of crack-propagation-induced ε-martensite in strain-controlled low-cycle fatigue of high-Mn austenitic steel. Philosophical Magazine Letters, 2015, 95, 303-311.	1.2	25
148	Effects of Si on Tensile Properties Associated with Deformation-Induced ε-Martensitic Transformation in High Mn Austenitic Alloys. Nippon Kinzoku Gakkaishi/Journal of the Japan Institute of Metals, 2015, 79, 657-663.	0.4	3
149	Effects of Si on Tensile Properties Associated with Deformation-Induced ε-Martensitic Transformation in High Mn Austenitic Alloys. Materials Transactions, 2015, 56, 819-825.	1.2	19
150	Characteristic Fatigue Crack Growth Behavior of Low Carbon Steel Under Low-pressure Hydrogen Gas Atmosphere in an Ultra-low Frequency. Tetsu-To-Hagane/Journal of the Iron and Steel Institute of Japan, 2015, 101, 605-610.	0.4	0
151	Notch Sensitivity in Fatigue Limit of High Strength Steel. Tetsu-To-Hagane/Journal of the Iron and Steel Institute of Japan, 2015, 101, 552-558.	0.4	1
152	Deformation Twinning Behavior of Twinning-induced Plasticity Steels with Different Carbon Concentrations – Part 2: Proposal of Dynamic-strain-aging-assisted Deformation Twinning. ISIJ International, 2015, 55, 1754-1761.	1.4	37
153	Detection of Charged Hydrogen in Ferritic Steel through Cryogenic Secondary Ion Mass Spectrometry. ISIJ International, 2015, 55, 335-337.	1.4	13
154	<i>ε</i> → <i>γ</i> Reverse Transformation-induced Hydrogen Desorption and Mn Effect on Hydrogen Uptake in Fe–Mn Binary Alloys. ISIJ International, 2015, 55, 2269-2271.	1.4	12
155	Intergranular Fatigue Crack Initiation and Its Associated Small Fatigue Crack Propagation in Water-quenched Fe–C Fully Ferritic Steel. ISIJ International, 2015, 55, 2463-2468.	1.4	19
156	Positive and negative effects of hydrogen on tensile behavior in polycrystalline Fe–30Mn–(6 â^'x)Si–xAl austenitic alloys. Scripta Materialia, 2015, 105, 54-57.	5.2	38
157	Effects of cementite morphology on short-fatigue-crack propagation in binary Fe–C steel. Philosophical Magazine Letters, 2015, 95, 384-391.	1.2	18
158	Effects of hydrogen-altered yielding and workÂhardening on plastic-zone evolution: AÂfinite-element analysis. International Journal of Hydrogen Energy, 2015, 40, 9825-9837.	7.1	23
159	Factors affecting hydrogen-assisted cracking in a commercial tempered martensitic steel: Mn segregation, MnS, and the stress state around abnormal cracks. Materials Science & Engineering A: Structural Materials: Properties, Microstructure and Processing, 2015, 640, 72-81.	5.6	37
160	Tensile properties of precracked tempered martensitic steel specimens tested at ultralow strain rates in high-pressure hydrogen atmosphere. Philosophical Magazine Letters, 2015, 95, 260-268.	1.2	15
161	An Overview of Dual-Phase Steels: Advances in Microstructure-Oriented Processing and Micromechanically Guided Design. Annual Review of Materials Research, 2015, 45, 391-431.	9.3	469
162	Spatially and Kinetically Resolved Mapping of Hydrogen in a Twinning-Induced Plasticity Steel by Use of Scanning Kelvin Probe Force Microscopy. Journal of the Electrochemical Society, 2015, 162, C638-C647.	2.9	64

#	Article	IF	CITATIONS
163	Enhancing Hydrogen Embrittlement Resistance of Lath Martensite by Introducing Nano-Films of Interlath Austenite. Metallurgical and Materials Transactions A: Physical Metallurgy and Materials Science, 2015, 46, 3797-3802.	2.2	77
164	Deformation Twinning Behavior of Twinning-induced Plasticity Steels with Different Carbon Concentrations – Part 1: Atomic Force Microscopy and Electron Backscatter Diffraction Measurements. ISIJ International, 2015, 55, 1747-1753.	1.4	8
165	Suppression Mechanism of Strain-age Hardening in Carbon Steel Associated with Hydrogen Uptake. Tetsu-To-Hagane/Journal of the Iron and Steel Institute of Japan, 2015, 101, 546-551.	0.4	1
166	Hydrogen Embrittlement in Al-Added Twinning-Induced Plasticity Steels Evaluated by Tensile Tests during Hydrogen Charging. Tetsu-To-Hagane/Journal of the Iron and Steel Institute of Japan, 2014, 100, 662-667.	0.4	0
167	Factors Affecting Static Strain Aging Under Stress at Room Temperature in a Fe-Mn-C Twinning-Induced Plasticity Steel. Tetsu-To-Hagane/Journal of the Iron and Steel Institute of Japan, 2014, 100, 1123-1131.	0.4	2
168	Deformation Twinning Behavior of Twinning-Induced Plasticity Steels with Different Carbon Concentrations. Tetsu-To-Hagane/Journal of the Iron and Steel Institute of Japan, 2014, 100, 1253-1260.	0.4	6
169	Deformation Twinning Behavior of Twinning-Induced Plasticity Steels with Different Carbon Concentrations. Tetsu-To-Hagane/Journal of the Iron and Steel Institute of Japan, 2014, 100, 1246-1252.	0.4	8
170	Alloy Design, Combinatorial Synthesis, and Microstructure–Property Relations for Low-Density Fe-Mn-Al-C Austenitic Steels. Jom, 2014, 66, 1845-1856.	1.9	172
171	Tensile Testing with Cyclic Strain Holding to Analyze Dynamic Recrystallization of Pure Lead. Advances in Materials Science and Engineering, 2014, 2014, 1-8.	1.8	2
172	Hydrogen-assisted decohesion and localized plasticity in dual-phase steel. Acta Materialia, 2014, 70, 174-187.	7.9	366
173	Strain mapping with high spatial resolution across a wide observation range by digital image correlation on plastic replicas. Materials Characterization, 2014, 98, 140-146.	4.4	30
174	Hydrogen embrittlement associated with strain localization in a precipitation-hardened Fe–Mn–Al–C light weight austenitic steel. International Journal of Hydrogen Energy, 2014, 39, 4634-4646.	7.1	170
175	Effects of Static and Dynamic Strain Aging on Hydrogen Embrittlement in TWIP Steels Containing Al. Tetsu-To-Hagane/Journal of the Iron and Steel Institute of Japan, 2014, 100, 1132-1139.	0.4	5
176	Hydrogen-assisted quasi-cleavage fracture in a single crystalline type 316 austenitic stainless steel. Corrosion Science, 2013, 75, 345-353.	6.6	85
177	Grain refinement effect on cryogenic tensile ductility in a Fe–Mn–C twinning-induced plasticity steel. Materials & Design, 2013, 49, 234-241.	5.1	61
178	Microstructure characteristic and its effect on mechanical and shape memory properties in a Fe–17Mn–8Si–0.3C alloy. Journal of Alloys and Compounds, 2013, 573, 15-19.	5.5	6
179	Hydrogen-assisted failure in a twinning-induced plasticity steel studied under in situ hydrogen charging by electron channeling contrast imaging. Acta Materialia, 2013, 61, 4607-4618.	7.9	218
180	TWIP Effect and Plastic Instability Condition in an Fe^ ^ndash;Mn^ ^ndash;C Austenitic Steel. ISIJ International, 2013, 53, 323-329.	1.4	67

#	Article	IF	CITATIONS
181	Factors Affecting Static Strain Aging under Stress at Room Temperature in a Fe–Mn–C Twinning-induced Plasticity Steel. ISIJ International, 2013, 53, 1089-1096.	1.4	9
182	Effects of Static and Dynamic Strain Aging on Hydrogen Embrittlement in TWIP Steels Containing Al. ISIJ International, 2013, 53, 1268-1274.	1.4	24
183	Inverse grain size dependence of critical strain for serrated flow in a Fe–Mn–C twinning-induced plasticity steel. Philosophical Magazine Letters, 2012, 92, 145-152.	1.2	19
184	Hydrogen Embrittlement in Al-added Twinning-induced Plasticity Steels Evaluated by Tensile Tests during Hydrogen Charging. ISIJ International, 2012, 52, 2283-2287.	1.4	35
185	Influence of Dislocation Separation on Dynamic Strain Aging in a Fe–Mn–C Austenitic Steel. Materials Transactions, 2012, 53, 546-552.	1.2	29
186	Selective appearance of <i>ϵ</i> -martensitic transformation and dynamic strain aging in Fe–Mn–C austenitic steels. Philosophical Magazine, 2012, 92, 3051-3063.	1.6	28
187	Hydrogen embrittlement in a Fe–Mn–C ternary twinning-induced plasticity steel. Corrosion Science, 2012, 54, 1-4.	6.6	134
188	Effect of hydrogen content on the embrittlement in a Fe–Mn–C twinning-induced plasticity steel. Corrosion Science, 2012, 59, 277-281.	6.6	103
189	Effect of deformation temperature on tensile properties in a pre-cooled Fe–Mn–C austenitic steel. Materials Science & Engineering A: Structural Materials: Properties, Microstructure and Processing, 2012, 556, 331-336.	5.6	12
190	Premature Fracture Mechanism in an Fe-Mn-C Austenitic Steel. Metallurgical and Materials Transactions A: Physical Metallurgy and Materials Science, 2012, 43, 4063-4074.	2.2	52
191	Quasi-cleavage Fracture along Annealing Twin Boundaries in a Fe–Mn–C Austenitic Steel. ISIJ International, 2012, 52, 161-163.	1.4	31
192	Tensile deformation behavior of Fe–Mn–C TWIP steel with ultrafine elongated grain structure. Materials Letters, 2012, 75, 169-171.	2.6	69
193	Hydrogen-induced cracking at grain and twin boundaries in an Fe–Mn–C austenitic steel. Scripta Materialia, 2012, 66, 459-462.	5.2	168
194	Hydrogen-induced delayed fracture of a Fe–22Mn–0.6C steel pre-strained at different strain rates. Scripta Materialia, 2012, 66, 947-950.	5.2	50
195	Work hardening and uniform elongation of an ultrafine-grained Fe–33Mn binary alloy. Materials Science & Engineering A: Structural Materials: Properties, Microstructure and Processing, 2011, 530, 659-663.	5.6	16
196	Nanoindentation/atomic force microscopy analyses of ε-martensitic transformation and shape memory effect in Fe–28Mn–6Si–5Cr alloy. Scripta Materialia, 2011, 65, 942-945.	5.2	43
197	Si content dependence on shape memory and tensile properties in Fe–Mn–Si–C alloys. Materials Science & Engineering A: Structural Materials: Properties, Microstructure and Processing, 2011, 528, 2882-2888.	5.6	40
198	Work hardening associated with É≻martensitic transformation, deformation twinning and dynamic strain aging in Fe–17Mn–0.6C and Fe–17Mn–0.8C TWIP steels. Materials Science & Engineering A: Structural Materials: Properties, Microstructure and Processing, 2011, 528, 7310-7316.	5.6	185

#	Article	IF	CITATIONS
199	Continuous Transition of Deformation Modes in Fe-30Mn-5Si-1Al Alloy. Materials Transactions, 2010, 51, 1194-1199.	1.2	8
200	Continuous Transition of Deformation Mode in Fe-30Mn-5Si-1Al Alloy. Nippon Kinzoku Gakkaishi/Journal of the Japan Institute of Metals, 2009, 73, 174-179.	0.4	4
201	The effects of thermomechanical training treatment on the deformation characteristics of Fe–Mn–Si–Al alloys. Materials Science & Engineering A: Structural Materials: Properties, Microstructure and Processing, 2008, 497, 353-357.	5.6	42
202	Mechanism of reversible transformation-induced plasticity of Fe–Mn–Si shape memory alloys. Scripta Materialia, 2008, 59, 826-829.	5.2	91
203	AFM Observation of Microstructural Changes in Fe-Mn-Si-Al Shape Memory Alloy. Materials Transactions, 2008, 49, 812-816.	1.2	14
204	Atomic Force Microscopic Observation of Microstructural Changes in Fe-Mn-Si-Al Shape Memory Alloy. Nippon Kinzoku Gakkaishi/Journal of the Japan Institute of Metals, 2007, 71, 672-677.	0.4	4
205	Influence of Al on Shape Memory Effect and Twinning Induced Plasticity of Fe-Mn-Si-Al System Alloy. Nippon Kinzoku Gakkaishi/Journal of the Japan Institute of Metals, 2007, 71, 502-507.	0.4	6
206	Influence of Al on Shape Memory Effect and Twinning Induced Plasticity of Fe-Mn-Si-Al System Alloy. Materials Transactions, 2007, 48, 2729-2734.	1.2	27
207	Investigation on Mode I Propagation Behavior of Fatigue Crack in Precipitation-Hardened Aluminum Alloy with Different Mg Content. Materials Science Forum, 0, 889, 143-147.	0.3	2